Gaussian Mixture Model based Convolutional Sparse Coding for Radar Heartbeat Detection

Jingwei Liu*, J. Andrew Zhang*, Richard Xu*, Andre Pearce*, Wei Ni†, Mark Hedley†
* School of Electrical and Data Engineering, University of Technology Sydney, Australia
†Cyber Physics Program, Data61, CSIRO, Australia
Correpsonding Email: Jingwei.Liu-1@student.uts.edu.au; Andrew.Zhang@uts.edu.au

***Abstract*—Accurate detection of heartbeat through radar has many potential applications in, e.g., security and health. However, it is generally challenging to obtain clear heartbeat signature, due to its weak signal and relatively large interference caused by, e.g., body and respiration movement. In this paper, we propose an advanced algorithm based on convolutional sparse coding (CSC) and Gaussian mixture model (GMM) for suppressing the interference and extracting clear heartbeat signals. In this study, heartbeat signals are modelled by CSC and recovered by exploiting the sparsity of the signal. GMM is introduced to model the unknown noise, which could be a mixture from multiple noise/interference sources. The parameters of GMM , dictionary and codes are computed via the expectation maximization (EM) algorithm. To achieve faster processing, convolution computing is proposed to be processed in the frequency domain. The proposed method is tested and validated by simulation and experiments. The results show that our proposed algorithm can accurately extract the heartbeat components.**

***Index Terms*—Heartbeat Detection , FMCW Radar, Gaussian Mixture Model, Accelerated Proximal Gradient Descent**

I. Introduction

Heartbeat rate (HR), is a critical physiological parameter of human body, that is desired in smart home, life detection, and medical applications. Traditional methods for obtaining heartbeats is using contact equipment like ECG. Contact equipment can get accurate measurements, however, its usage may cause inconvenience to users, and sometimes users may be in inaccessible locations. Therefore noncontact devices such as radar are great alternative options. Radar has been used in, e.g., monitoring infant heart disease and for observing important human physiological parameters related to multiple kinds of diseases. In these applications, tiny displacements caused by vital signs can be detected by observing peak phases in the frequency domain. The larger the bandwidth of the radar signal is, the better the resolution capability is.

Research on noncontact vital sign measurement can be traced back to 1970s [1]. Many efforts have been devoted to improving the sensing accuracy and detection range [2] since then. The arctangent demodulation [3] and adaptive DC calibration [4] based on continuous-wave (CW) radar extract primarily the Doppler frequency information. The micro-Doppler information is also utilized in the time-frequency domain [5]. Besides, assisting devices are designed to improve the accuracy of pattern extraction and cancel the interference caused by random body movement (RBM) or random system movement (RSM), such as deep camera [6], extra transceiver antenna pairs [7], and hybrid camera-radar system [8]. These traditional techniques typically transfer the reflected radar signals to other domains and apply parameter estimation.

Recently, more advanced techniques have been investigated to handle heartbeat extraction using radar in more challenging environment, e.g., in the presence of large interference and noise. Such noise largely affects the stability of many proposed algorithms. High demand for experiment parameters and the requirement of high-SNR data limit their applications [9] [10]. For example, the cubic polynomial fitting method in [11] reduces the accuracy of detection and the capability of processing low-SNR data allows noises caused by 20 mm/s random body movement at most, which is hard to control in experiment. The empirical mode decomposition(EMD) [10] and ensemble empirical mode decomposition (EEMD) [9] are introduced to cancel the high frequency artifacts. The periodicity of heartbeats are exploited by using the cyclostationary function [12]. The matched filter is used to deal with data obtained at low signal-to-noise ratio (SNR) [11].

The amplitude of heartbeat movement is typically much smaller compared to respiration and other movements, which makes heartbeat detection under noisy environment particularly challenging [13]. In [14], convolutional sparse coding (CSC) is introduced to detect heart beat rates. The sparse characteristics of heartbeats in the time domain can be utilized to separate them from noise by sparse decomposition and rebuild algorithms. As an unsupervised machine learning algorithm, CSC has been widely utilized in image processing, motion recognition, trajectories analysis and audio signal processing. Unsupervised machine learning requires few parameters, so this algorithm can be adaptive to environment variations. Compared with other algorithms, CSC works without requiring complicated parameter configuration.

In this paper, we improve the CSC scheme by introducing the Gaussian Mixture Model (GMM) to model noises, including device noise and environmental interferences, in heartbeats detection. Due to the square loss function, con-

ventional CSC algorithms generally utilize Gaussian model to model noises, which may not reflect the real noises in data. Actually, noises in measurement signals can be caused by, e.g., movement of tiny animals, environments, human body small movements and system itself, and its statistical distribution can be complicated [15]. Compared with existing methods, our GMM-CSC method uses less parameters, which makes training simpler, while improving system performance.

The rest of this paper is organized as follows. Section II describes data collection and pre-processing, to make the data ready for further CSC processing. Section III describes the proposed GMM-CSC scheme. Simulation and experimental results are presented in Section IV. Section V concludes the paper.

II. Data Collection and Pre-Processing

This section describes the principle of using FMCW radar for heartbeat collection, and the pre-processing modules to make the data ready for input to GMM-CSC.

A. FMCW Radar for Signal Collection

We use a FMCW radar operating at 60-64 GHz for collecting signals containing heartbeat information, with details to be provided in Section IV.

In an FMCW radar system, the transmitter sends the following chirp signals:

$$s_t = \sin(\omega_t t + \phi_t) \tag{1}$$

where ω_t represents frequency and ϕ is the initial phase. The frequency ω changes with time as $\omega_t = S*t+f_c, 0 \geq t \leq T_c$ where f_c is start frequency, S is the slope and T_c is the duration.

The FMCW radar captures the signals reflected by objectives in its propagation paths as $s_r = \sin(\omega_r t + \phi_r)$. The IF signal after the frequency mixer is

$$s_{IF} = \sin((\omega_t - \omega_r)t + \phi_t - \phi r). \tag{2}$$

The initial phase of the IF signal can be expressed as the difference between the initial phases of the received and transmitted signals. Since the initial phase of the received signal is fixed, the initial phase of the IF signal is determined by the arrival time of the transmitted signal. Chest vibration caused by vital signs may result in a slight change in the length of the propagation path. Therefore, heartbeats can be determined by observing the peak phase in the frequency domain. The relationship between distance d and phase Φ can be represented as $\Phi = 2\pi f_c \tau = \frac{4\pi d}{\lambda}$ where τ is the arrival time delay caused by d and λ is the wavelength.

B. System Structure and Pre-Processing

The structure of the system is shown in Fig. 1. It includes the following modules:

- Beat signal extraction: Extract the vibration information of the target;

Fig. 1: System structure and signal pre-processing.

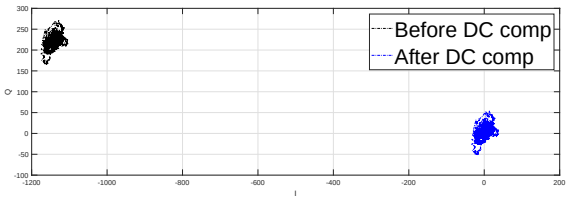

Fig. 2: Constellation correction of the received complex signal

- ADC: Convert raw continuous data to digital;
- Range FFT: Obtain the raw phase from the peak in every short-time matrix;
- DC compensation: Improve the quality of signals by compensating the DC component;
- Phase unwrapping: Unwrap phase for continuous displacement information; and
- GCSC: The module runs the GMM-CSC algorithm.

The operation of extracting the phase information from raw ADC data is elaborated as follows, referring to Fig. 1. After sampling N points from the single chirp, the range-FFT is applied for complex range profile. Repeat this for M chirps a $range - slow\ time$ matrix of size $M \times N$ is constructed. Each row of the matrix contains the information of the target at a certain time. The position of the peak in each line represents the distance between the target and the radar, and the number of peaks is corresponding to the number of objects. The small displacement change, including heartbeats, is reflected in the phase of peak value. Before obtaining the angle of the complex data, it is necessary to ensure that any non-linearity, distortion and artifacts have been eliminated. The phase calculation is highly non-linear, which increases the complexity of eliminating these defects. One method to improve phase quality is DC compensation. DC terms due to reasons rather than chest motions, for example the linkage form TX to RX, will affect the accuracy of phase. Fig.2 shows an example, where there is an apparent shift before DC compensation. In this paper, columns in $range - slow\ time$ matrix are presented in a I-Q axis. The DC component can be estimated by calculating the center of the point cloud data. After DC compensation the phases of each column in $range - slow\ time$ matrix is wrapped in $[-\pi, \pi]$. In contrast, the physical displacement may change beyond $\lambda/4$ (for a radar with frequency 60 GHz to 64 GHz, $\lambda/4$ is 1.25mm). Thus the phase may change beyond $[-\pi, \pi]$. The detailed unwrapping operation is referred to [16]. After DC compensation and phase-unwrapping, the phase data is now ready for GMM-CSC processing.

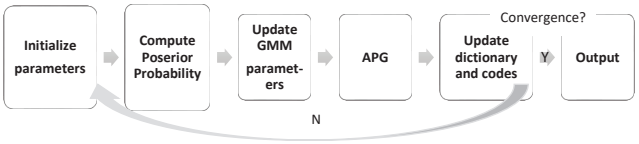

Fig. 3: Structure of GCSC

III. CSC WITH MIXED GAUSSIAN NOISE

This section presents the proposed GMM-CSC algorithm in detail, based on modeling the noises with GMM. In the first subsection, we use the expectation maximization (EM) algorithm for deriving the parameters of the GMM model. In the second subsection, via adding a regular term, we translate the M-step into a traditional CSC problem. We then use a mature and accelerated optimization algorithm to solve this problem.

The main steps of the method are as follows, as represented in Fig. 3.

1) Initialize parameters;
2) Compute the posterior probability (the E-step);
3) Update the GMM parameters (one part of the M-step): update covariance matrix to maximize the expectation;
4) Accelerated Proximal Gradient (APG) (another part of M-step): Update the dictionary and codes by solving a CSC problem;
5) Go back to the second step, until the maximum iterations are reached;
6) Output the de-noised signal.

In the beginning of the algorithm, random initial values of the dictionary and GMM parameters (the number of Gaussian components G, covariance matrix Σ_g, and weight π_g) are given. The posterior probability of the mixture can be obtained by the Bayesian equation. In the M-step we compute the derivative of the posterior probability to update the GMM parameters. A fast proximal gradient is used to update the dictionary and codes [17].

1) GMM and the EM Algorithm: The distance information Y we obtained can be presented as:

$$Y_i = \sum_{k=1}^{Dm} d_k * z_{ik} + \varepsilon_i, \tag{3}$$

where i presents the ith sample and d_k and z_{ik} represent the element and corresponding codes, respectively. We can compute N samples at one time so $i \leq N$; ε_i is the combined noise caused by multiple factors as discussed before. Assume that noise N_i is a sample from a GMM distribution with probability density function (pdf)

$$p(\varepsilon) \sim \sum_{g=1}^{G} \pi_g N(\varepsilon|0, \Sigma_g), \tag{4}$$

where G is the total number of Gaussian components.

The EM algorithm can be used to estimate the parameters that maximize the likelihood function of the GMM. We define a latent variable $\phi_{ik} \in 0, 1$, which indicates the assignment of the noise in the ith data to the kth Gaussian noise. From [15] we can get the log posterior probability as:

$$E(\phi_{ig}) = \frac{\pi_g N(Y_i|\sum_{k=1}^{K} d_k * z_{ik}, \Sigma_g)}{\sum_{m=1}^{G} \pi_m N(Y_i|\sum d_k * z_{ik}, \Sigma_m)} = \gamma_{ig}. \tag{5}$$

Then the E-step is completed as

$$E(Y, \phi|\pi, D, z, \Sigma) = \sum_{i=1}^{N}\sum_{g=1}^{G} \gamma_{ig}(\log \pi_g - \frac{1}{2} log(|\Sigma_g|) - \frac{1}{2}\frac{(Y_i - \sum_{k=1}^{K} d_k * z_{ik})^2}{\Sigma_g}). \tag{6}$$

We can take derivation of (6) to maximum the upper bound:

$$\pi_g = \frac{1}{N}(\sum_{i=1}^{N} \gamma_{ig}); \tag{7}$$

$$\Sigma_g = \frac{\sum_{i=1}^{N} \gamma_{ig}(Y_i - \sum_{k=1}^{K} d_k * z_{ik})^\top (Y_i - \sum_{k=1}^{K} d_k * z_{ik})}{\sum_{i=1}^{N} \gamma_{ig}}. \tag{8}$$

From (7) we can update the sets π_g and Σ_g for every sample. After removing the updated parameter, the maximum of (6) is

$$\max \sum_{i=1}^{N}\sum_{g=1}^{G} \gamma_{ig}(-\frac{1}{2}\frac{(Y_i - \sum_{k=1}^{K} d_k * z_{ik})^2}{\Sigma_g}), \tag{9}$$

which is equal to an optimization problem

$$\min \sum_{i=1}^{N}\sum_{g=1}^{G} \gamma_{ig}(\omega_{gi}(Y_i - \sum_{k=1}^{K} d_k * z_{ik})^2), \tag{10}$$

where $\omega_{gi}(P) = \frac{\gamma_{ig}}{\sigma_g^2(P)}$. In order to ensure the sparsity of codes z we can add a Lasso regularization part to (10) as

$$\min \sum_{i=1}^{N}\sum_{g=1}^{G} \gamma_{ig}(\omega_{gi}(Y_i - \sum_{k=1}^{K} d_k * z_{ik})^2) + \beta\|z_{ik}\|_1 \tag{11}$$

If we separate the function into two parts: $F = f + r$ where $f = \frac{1}{2}\sum_{i=1}^{N}\sum_{g=1}^{G}\|w_{gi} \odot (Y_i - \sum d_k * z_{ik})\|_F^2$ and $r = \sum_{k=1}^{K} \beta\|z_{ik}\|_1 + I_D(d_k)$. With (w_{gi}) known we can treat F as a weighted CSC problem.

2) CSC: We choose the accelerate proximal gradient (APG) method to solve the CSC problem. APG and its variances are one of the best methods for solving non-smooth optimization problems. Almost all APG algorithms can reach the convergence rate of $O(1/k)$. We can update d_k and z_{ik} by using APG. The APG algorithm is summarized in Algorithm 1. Using the outputs from the algorithm we can update d_k and z_{ik}.

IV. SIMULATION AND EXPERIMENTAL RESULTS

In this section, we provide simulation and experimental results to validate the efficiency of the proposed GMM-CSC scheme. We first use artificially generated data to simulate

Algorithm 1 The APG Algorithm

input: D,z,J,λ,β,$t^0 = t^1 = 1$,η
  for j=1,...,J **do**
    u_k^j=$d_k^j + \frac{t^{k-1}-1}{t^k}(d_k^j - d_k^{j-1})$ for all k
    v_k^j=$d_k^j + \frac{t^{k-1}-1}{t^k}(z_k^j - z_k^{j-1})$for all k
    for i=1,2,... **do**
      $a^0 = \eta * b^{k-1}$
      d_k^{j+1}=$prox_{\eta I_D}(u_k^j - (a^j)^{-1}\frac{\partial f(d_k,z_{ik})}{\partial d_k})$
      z_k^{j+1}=$prox_{\beta\eta\|\|_1}(v_k^j - (a^j)^{-1}\frac{\partial f(d_k,z_{ik})}{\partial z_{ik}})$
      if $F(d_k^j, z_k^j) \geq F(d_k^{j-1}, z_k^{j-1})$ **then**
        $b^k = a^j$
      else$a^{j+1} = \eta^{-1} * a^j$
      end if
    end for
    d_k^{j+1}=$prox_{\eta I_D}(u_k^j - (a^j)^{-1}\frac{\partial f(d_k,z_{ik})}{\partial d_k})$
    z_k^{j+1}=$prox_{\beta\eta\|\|_1}(v_k^j - (a^j)^{-1}\frac{\partial f(d_k,z_{ik})}{\partial z_{ik}})$
    $t^{k+1} = \frac{1+\sqrt{1+4*t^k}}{2}$
  end for
  Return d_k^{j+1}, z_{ik}^{j+1}

some heartbeat for testing. We then conduct experiments using practically collected data with an FMCW radar. In both simulation and experiments, only the step length (for optimization) and the regularization parameter require adjustment. Our proposed GMM-CSC method is compared to the known normal CSC algorithm and the one with applying a low-pass filter.

A. Simulation

We first construct a clean signal, which is composed of a respiratory signal with a frequency of 0.5 and an amplitude of 1.5, and a heartbeat signal with a frequency of 1 and an amplitude of 0.2. We mixed five types of noise, as shown in Table I. In the simulation the number of elements is set as 12 and each element has a length OF 30 points. There are 200 points in the signal so the length of codes used in CSC is 171. The step size of every iteration are fixed and the number of iteration are set as 50 times.

The simulation results for different methods are shown in Fig. 4. Fig. 4a and Fig.4b show the original signal we create and the signal with added mixed noises. Fig.4c to Fig 4e show the results of applying three processing methods.

Fig. 4c shows the result of processing the signal with a low-pass filter. The high frequency component of noise is eliminated, however the low frequency component that is close to the vital sign frequency is not removed. Fig. 4d and Fig. 4e are the signals obtained by using normal CSC and CSC with GMM. Our proposed GMM-CSC demonstrates improved performance. Firstly, the frequency domain spectrum obtained by the normal CSC always contains components which do not belong to the original signal 5. Secondly, as shown in Table II, the deviation of estimation for the normal CSC is about 50% more than that for GMM-CSC.

Noise Composition	Distribution
Guassian	$\mathcal{N}(0, 0.1)$
Laplace	$1.5 * \mathcal{L}(0, 0.8)$
Gaussian	$\mathcal{N}(0, 0.3)$
Gaussian	$\mathcal{N}(0, 0.7)$
Gaussian	$\mathcal{N}(0, 1)$

TABLE I: Parameters of different distributions.

Methods	Deviation
Low-pass filter	22.3731
Normal CSC	12.6231
CSC with GMM	8.2225

TABLE II: Results of different methods.

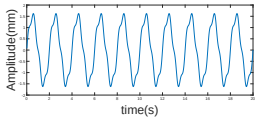

(a) Original simulated signal.

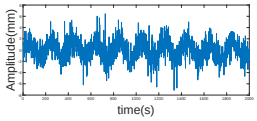

(b) Signal with mixed noises.

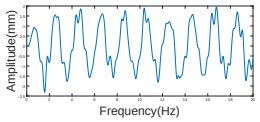

(c) Result of using low-pass filter.

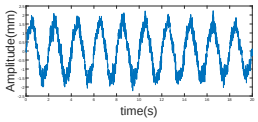

(d) Result of normal CSC algorithm.

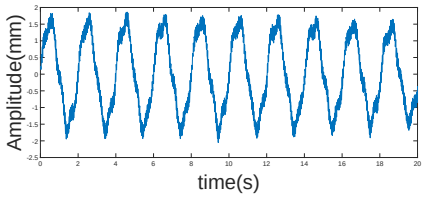

(e) Result of CSC algorithm with GMM.

Fig. 4: Simulation result

B. Experimental Results

In the experiments, a Texas Instrument (TI) mm-wave radar (IWR6843) operating from 60 to 64 GHz is employed, and the maximal wavelength (at the 60 GHz band) is 4.99 mm. The frame period is 40 ms and there are 128 chirps per frame. The sampling rate is 256 times per chirp. The maximal detection range is 2.14 m and the vibration frequency resolution is 0.0782 Hz. The vibration frequency of the chest for the heart rate is in the range of $[0.8, 2]$ Hz. For a typical adult, the amplitude of heartbeat is about 0.5 mm to 0.8 mm. Both frequencies and amplitudes of the heartbeat signal are within the acceptable range of the radar, thus they can be effectively detected.

Fig. 6 presents the initial scene setting for the experiment. The distance between the subject and radar is 50 cm at the beginning and step up 10 cm each time until 100 cm. The

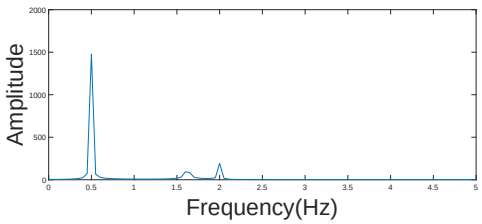

(a) Result of normal CSC in Frequency domain.

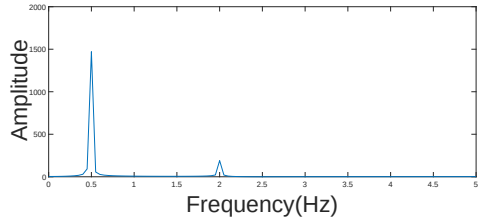

(b) Result of CSC with GMM in Frequency domain.

Fig. 5: CSC and GMM-CSC results in frequency domain.

Fig. 6: Scene setup for experiment.

length of collected data each time is also one of the important parameters. Though data collected over longer time can lead to higher frequency resolution, heartbeat rate always changes with time so it is not suitable to select data with a period of 30 s or longer, as mentioned in [18]. Additional algorithms adaptive to the variations of HR need to be further developed to allow continuous tracking. Here, signal data of approximately 5 seconds is used each time.

As shown in Fig 7, vibration caused by heartbeat is obvious. It is not feasible to obtain the heart rate directly from the unprocessed data because the heart rate in the frequency domain is interfered by respiratory harmonics and other noises.

A band-filter with band pass $[0.4, 5]$ is utilized to remove respiration component. The frequency spectrum obtained before and after applying the GMM-CSC algorithm are shown in Fig. 8a and Fig. 8b. Only principal components

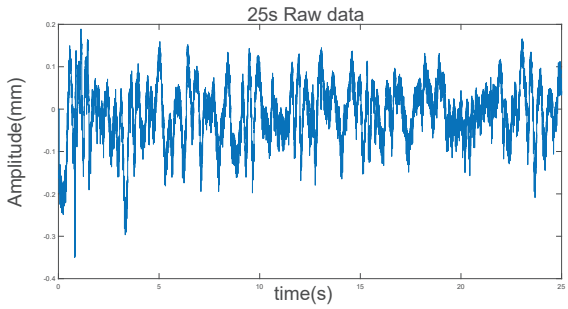

Fig. 7: unwrapped-phase signal with time period 25 seconds

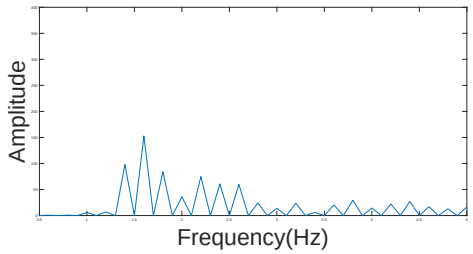

(a) Frequency domain spectrum before algorithm

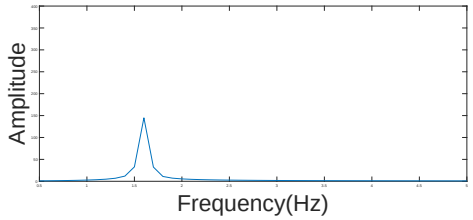

(b) Frequency domain after algorithm

Fig. 8: Change in frequency domain after GMM-CSC

are presented through adjusting the code sparsity and the main ingredient in frequency domain gather around one peak. The heartbeat spectrum is shown in Fig.9. the HR is approximately 1.6 Hz. Taking the limited resolution and leakage effect, the deviation is about ± 0.2 Hz. Results compared to other ones [16] [19] are presented in Table III.

Experiments on multiple targets were also conducted. Fig 10 shows the scene of the two-target experiments. From the range-FFT figure as shown in Fig. 11, two peaks can be separated easily. Phase information from two targets can then be extracted from two separated peaks and the results are

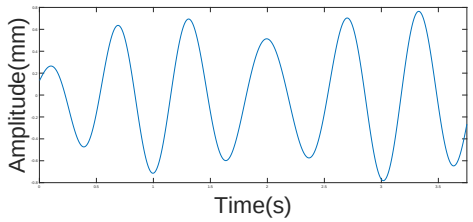

Fig. 9: Heartbeat signal extracted.

Ref.	Distance(m)	f_{min}(GHz)	Correct rate(HR)
[16]	1.7	77	0.80
[19]	1	80	0.87
Ours	1.6	60	about 0.88

TABLE III: Comparison with existing algorithms.

Fig. 10: Two-target experimental scene.

shown in Fig. 11. The figure indicates that vital signs for both people can be obtained. The distance between target 2 and radar is larger thus the heartbeat component extracted for target 2 is interfered.

V. Conclusions

In this paper, the GMM-CSC algorithm is proposed for suppressing the mixed noise in measured radar signals containing heartbeat information. Performance improvements in detecting heart rates are demonstrated via both simulation and experimental data. The algorithm is especially effective when processing phase signals that contain complex noise and less motion artifacts. The proposed method has the following advantages: (i) Simple unsupervised machine learning method, with very few parameters to adjust; and (ii) Strong robustness to noise. Future works include adaption to varying heartbeats and automatic separation of multi-target signals.

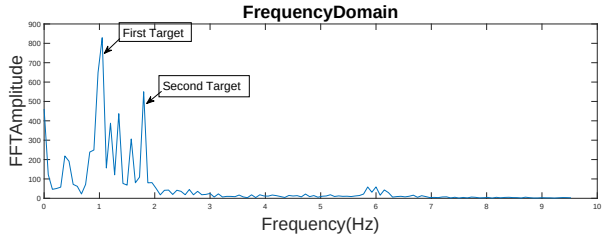

Fig. 11: Range-FFT figure.

References

[1] J. C. Lin, "Noninvasive microwave measurement of respiration," *Proceedings of the IEEE*, vol. 63, no. 10, pp. 1530–1530, 1975.

[2] C. Li, V. M. Lubecke, O. Boric-Lubecke, and J. Lin, "A review on recent advances in doppler radar sensors for noncontact healthcare monitoring," *IEEE Transactions on microwave theory and techniques*, vol. 61, no. 5, pp. 2046–2060, 2013.

[3] B.-K. Park, O. Boric-Lubecke, and V. M. Lubecke, "Arctangent demodulation with dc offset compensation in quadrature doppler radar receiver systems," *IEEE transactions on Microwave theory and techniques*, vol. 55, no. 5, pp. 1073–1079, 2007.

[4] X. Zhao, C. Song, V. Lubecke, and O. Boric-Lubecke, "Dc coupled doppler radar physiological monitor," in *2011 Annual International Conference of the IEEE Engineering in Medicine and Biology Society*. IEEE, 2011, pp. 1909–1912.

[5] T. Thayaparan, L. Stanković, and I. Djurović, "Micro-doppler-based target detection and feature extraction in indoor and outdoor environments," *Journal of the Franklin Institute*, vol. 345, no. 6, pp. 700–722, 2008.

[6] M. Papakostas, J. Staud, F. Makedon, and V. Metsis, "Monitoring breathing activity and sleep patterns using multimodal non-invasive technologies," in *Proceedings of the 8th ACM International Conference on PErvasive Technologies Related to Assistive Environments*, 2015, pp. 1–4.

[7] C. Li and J. Lin, "Random body movement cancellation in doppler radar vital sign detection," *IEEE Transactions on Microwave Theory and Techniques*, vol. 56, no. 12, pp. 3143–3152, 2008.

[8] C. Gu, G. Wang, Y. Li, T. Inoue, and C. Li, "A hybrid radar-camera sensing system with phase compensation for random body movement cancellation in doppler vital sign detection," *IEEE Transactions on Microwave Theory and Techniques*, vol. 61, no. 12, pp. 4678–4688, 2013.

[9] K. Shyu, L. Chiu, P. Lee, T. Tung, and S. Yang, "Detection of breathing and heart rates in uwb radar sensor data using fvpief-based two-layer eemd," *IEEE Sensors Journal*, vol. 19, no. 2, pp. 774–784, 2019.

[10] I. Mostafanezhad, E. Yavari, O. Boric-Lubecke, V. M. Lubecke, and D. P. Mandic, "Cancellation of unwanted doppler radar sensor motion using empirical mode decomposition," *IEEE Sensors Journal*, vol. 13, no. 5, pp. 1897–1904, 2013.

[11] Q. Lv, L. Chen, K. An, J. Wang, H. Li, D. Ye, J. Huangfu, C. Li, and L. Ran, "Doppler vital signs detection in the presence of large-scale random body movements," *IEEE Transactions on Microwave Theory and Techniques*, vol. 66, no. 9, pp. 4261–4270, 2018.

[12] S. Kazemi, A. Ghorbani, H. Amindavar, and C. Li, "Cyclostationary approach to doppler radar heart and respiration rates monitoring with body motion cancelation using radar doppler system," *Biomedical Signal Processing and Control*, vol. 13, pp. 79–88, 2014.

[13] S. Bakhtiari, S. Liao, T. Elmer, A. Raptis *et al.*, "A real-time heart rate analysis for a remote millimeter wave iq sensor," *IEEE transactions on biomedical engineering*, vol. 58, no. 6, pp. 1839–1845, 2011.

[14] P. Wang, F. Qi, M. Liu, F. Liang, H. Xue, Y. Zhang, H. Lv, and J. Wang, "Noncontact heart rate measurement based on an improved convolutional sparse coding method using ir-uwb radar," *IEEE Access*, vol. 7, pp. 158 492–158 502, 2019.

[15] Y. Wang, J. T. Kwok, and L. M. Ni, "Generalized convolutional sparse coding with unknown noise," *IEEE Transactions on Image Processing*, vol. 29, pp. 5386–5395, 2020.

[16] M. Alizadeh, G. Shaker, J. C. M. D. Almeida, P. P. Morita, and S. Safavi-Naeini, "Remote monitoring of human vital signs using mm-wave fmcw radar," *IEEE Access*, vol. 7, pp. 54 958–54 968, 2019.

[17] Q. Yao, J. T. Kwok, F. Gao, W. Chen, and T.-Y. Liu, "Efficient inexact proximal gradient algorithm for nonconvex problems," *arXiv preprint arXiv:1612.09069*, 2016.

[18] H. Shen, C. Xu, Y. Yang, L. Sun, Z. Cai, L. Bai, E. Clancy, and X. Huang, "Respiration and heartbeat rates measurement based on autocorrelation using ir-uwb radar," *IEEE Transactions on Circuits and Systems II: Express Briefs*, vol. 65, no. 10, pp. 1470–1474, 2018.

[19] S. Wang, A. Pohl, T. Jaeschke, M. Czaplik, M. Köny, S. Leonhardt, and N. Pohl, "A novel ultra-wideband 80 ghz fmcw radar system for contactless monitoring of vital signs," in *2015 37th Annual International Conference of the IEEE Engineering in Medicine and Biology Society (EMBC)*. IEEE, 2015, pp. 4978–4981.